ASSESSMENT OF A CAA METHODOLOGY FOR TURBULENCE-CASCADE INTERACTION NOISE PREDICTION AND REDUCTION FROM SERRATED AIRFOILS

Martin Buszyk[1,*] **Cyril Polacsek**[1] **Thomas Le Garrec**[1]

[1] ONERA, The French Aerospace Lab, Numerical Aeroacoustic Team, 92320 Châtillon, France.

[*] PhD student at the Ecole Centrale de Lyon, France - MEGA doctoral school.

`martin.buszyk@onera.fr`

ABSTRACT

The acoustic response of a rectilinear cascade subjected to a grid turbulence will be analysed experimentally in a laboratory facility at the Ecole Centrale de Lyon in the framework of the H2020 European project InnoSTAT (*https://cordis.europa.eu/project/id/865007*). On this occasion, several noise reduction treatments will be evaluated. Here, we focus on the numerical prediction of one treatment proposed by ONERA: serrated leading edges. We performed several parametric studies on the baseline (untreated) geometry to assess the optimal simulation features for accurate and time effective calculations. In this parametric study two geometries are considered, namely NACA asymmetric airfoils and flat plates at zero incidence. The broadband noise simulations are carried out using a CAA code solving the linearized Euler equations, coupled with a stochastic turbulence generation. A particular attention is paid to the synthetic turbulence for which different formulations are considered, aiming at finding the best suited model for the studied configuration. Numerical cascade response is compared to that of an isolated flat plate using an analytical solution based on the Amiet formulation. Finally, the most suited numerical set-up is applied to the low-noise cascade and acoustic performances of the designed serrations are assessed. The results are compared to an analytical method using the Wiener-Hopf technique, both showing close OAPWL reductions around 6 dB.

1. INTRODUCTION

The broadband noise emitted by the fan stage is expected to increase on the future UHBR turbofan engines. In order to cope with the hardening of the certification procedures and the local rules, several technologies for noise reduction have been studied, in particular for tackling the prevailing rotor-stator interaction (RSI) noise. A quite promissive one highly investigated by ONERA is the use of leading edge serrations. Moreover the physical mechanism behind the RSI noise has been widely studied analytically, numerically and experimentally. With regard to the experimental part, the first step of the H2020 InnoSTAT project consists in testing noise reduction technologies on a 7-airfoils rectilinear cascade at the Ecole Centrale de Lyon. This type of

configuration provides more flexibility regarding the measurements and the tailoring of the turbulence using suited shaped grids (in order to mimic an isotropic turbulent inflow). Due to the fact that the experimental campaign has not yet been conducted, the parameters used for the numerical simulations carried out in this study are indicative, although they should remain close to the final ones.

	Parameter	Value
Airfoil	shape	NACA7310
	chord	12 cm
	span L_z	20 cm
	vane spacing s	8.5 cm
Upstream flow U	norm	102 m· s^{-1}
	angle β_c	30°
Turbulent	Intensity TI	5 %
	Length Scale TLS	8 mm

Table 1: Main parameters of the rectilinear cascade.

The Tab. 1 sums up the main parameters used to simulate the experimental test facility which is illustrated in Fig. 1. The cascade consists in 7 evenly spaced NACA airfoils. The incoming turbulence is generated upstream of the cascade by means of a grid. Additional data about the experimental facility can be found in [1].
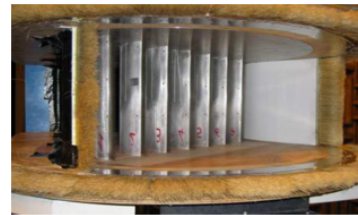

Figure 1: Picture of the rectilinear cascade facility [1].

Ahead of the planned experimental campaigns, the broadband noise predictions are forecasted through CAA (Computational Aero-Acoustics) simulations. The numerical methodology used here, is based on a synthetic turbulence approach implemented in a 3D in-house code, sAbrinA, which solves the perturbed Euler equations [2–4]. The synthetic turbulence is generated during the preprocessing as a set of Fourier modes as described in

the stochastic turbulence modelling initially introduced by Kraichnan [5] and continued by Bechara and Bailly [6]. The gusts are injected at the domain inlet (through a Tam's boundary condition) and convected by a mean flow field. The latter, currently obtained from a RANS calculation, is preferably computed by means of an open source Euler code [7] in order to satisfy the unviscous assumptions of the CAA. As regards the comparison of the results with the theory, analytical predictions are proposed too. In the first instance, the Amiet's isolated-airfoil response function [8] will serve as a common reference for the untreated (baseline) configurations. It should be noted that the literature provides several models accounting for the acoustic interaction of adjacent vanes, namely cascade effect [9]. However, these models have not been implemented as part of this study. As for the acoustic response of serrated vanes, an analytical approach based on the Wiener-Hoph technique [10] has been implemented on MATLAB (with an extension taking into account a finite span [4]).

2. ONE CHANNEL NUMERICAL SIMULATIONS

2.1 CAA numerical set up

The first set of simulations is performed on a single channel geometry ($s = L_y = 8.5$ cm) in order to limit the CPU time. Therefore, adjacent vanes are taken into account using periodic boundary conditions.
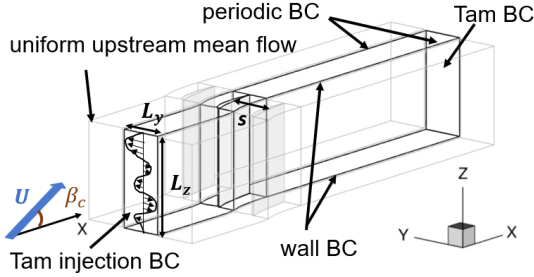

Figure 2: CAA set-up used for the simulation.

The CAA mesh sizing is chosen following some criteria from previous studies [2]. In particular, the space discretisation ensure at least 10-12 points per wavelength in all directions in which gusts are injected. Moreover, the grid density was chosen in order to limit the energy loss in the injected velocity spectrum to less than 1dB/Hz (only the gusts which are not noticeably dissipated by the mesh are injected). The CAA set-up (Tab. 2) is sketched in Fig. 2.
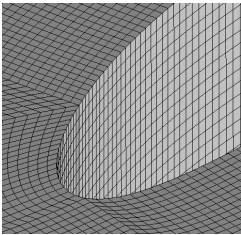

Figure 3: CAA mesh at the leading edge.

Parameter	Value
Δx_{max}	$8.5 \cdot 10^{-4}$ m
Δy_{max}	$4.3 \cdot 10^{-4}$ mm
Δz_{max}	$5.6 \cdot 10^{-4}$ m
$\Delta x, y, z_{min}$	$\approx 4.0 \cdot 10^{-4}$ m
Δt	$5.0 \cdot 10^{-7}$ s
f_{max}	10 kHz

Table 2: Numerical parameters.

Thereafter, a stretching zone is added at the exit of the domain coupled with a laplacian filter to dissipate the hydrodynamic fluctuations impinging the exit boundary condition. The H-type pattern with a leading edge split is chosen in order to define the blocking. The mesh is designed to tolerate gusts of frequencies up to 10 kHz. The time step is chosen in order to ensure a CFL number lower than 0.8. A local view of the 3D grid is shown in Fig. 3. The mesh has a total point number of 42 million.

2.2 Mean flow computation

The mean flow simulation is performed using an open source 2D Euler code [7]. This was justified by numerical issues that occur when using a RANS-based mean flow, particularly in the presence of serrations [4]. The required inputs are the total pressure and the total temperature at the inlet and the static pressure at the outlet. The surrounding conditions at rest are the atmospheric pressure and a static temperature equal to 20 °C. Two iterative procedures are needed in order to determine the angle of attack and the static pressure at the outlet. Giving a prescribed flow angle (between U and x axis) of 30°, the angle of attack is adjusted to a suited value of 9°, in order to give a roughly axial mean flow at the exit with respect to the behaviour of a turbofan stator stage. The static pressure at the outlet is tuned step by step in order to achieve the convergence of the flow rate at the entrance and therefore the desired Mach number. The H-pattern grid used here is obtained from a dedicated meshing tool provided with the CFD code. Fig. 4 illustrates the final iteration of the mean flow computation.
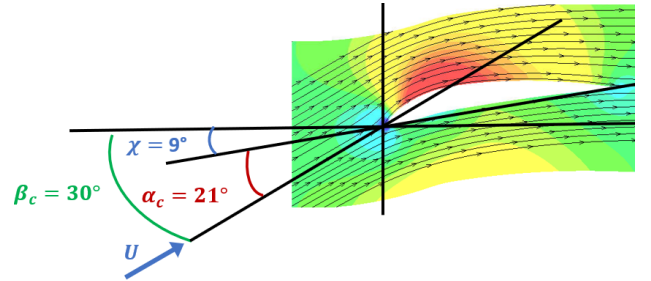

Figure 4: u'_x [m·s^{-1}] (levels between 60 and 120).

Contrary to a RANS mean flow, it is not necessary to perform a post-treatment of the mean flow. Indeed, the solution provided by the Euler code is free of recirculation zones and boundary layers that are incompatible with the hypothesis of the Euler equations implemented within the CAA code. Note that this Euler code has been also applied to the NASA SDT case and was found able to provide features with acceptable deviations (for CAA purpose) compared to RANS solutions.

2.3 Synthetic turbulence

The CFD Euler computation does not provide any information on the synthetic properties, which is not a limitation in the scope of this study because the turbulence properties are arbitrarily chosen (Tab. 1) and then fulfilled ex-

perimentally by an adequately designed turbulence grid. The parameters chosen here are representative of previous studies and could be tuned thereafter. In line with the previous studies carried out at ONERA on the stochastic turbulence [3, 4, 11], the Fourier-mode decomposition was adapted to an annular cascade problem with a swirling mean flow, and practically achieved by considering a 1-wavenumber, 2-wavenumber, or 3-wavenumber isotropic turbulence spectrum model, focused to the upwash component (by analogy with Amiet's theory). For that, the latest generation and post-processing codes in annular geometry have been rewritten into cartesian coordinates. Meanwhile, a computer optimization of the Fortran routines has allowed a gain of about 20 on the time needed for the generation of the synthetic turbulence. The latter is described by the Eqn. (1) and Eqn. (2) with $\varphi_{\eta\eta}$ the Liepmann autocorrelation spectrum of the upwash velocity u'_η (and ψ a random phase).

$$\begin{cases} u'_y = \sum_{l=1}^{L} A_l \cos(k_{\xi,l}(\xi\text{-}Ut)+\psi_l) \\ A_l = \dfrac{2}{\cos(\beta_c)}\sqrt{\varphi_{\eta\eta}^{2D}(k_{\xi,l},k_z=0)\Delta k_\xi \Delta k_z} \end{cases} \quad (1)$$

$$\begin{cases} u'_y = \sum_{l=1}^{L}\sum_{n=\text{-}N}^{N} A_{ln}\cos(k_{\xi,l}(\xi\text{-}Ut)+k_{z,n}z+\psi_{ln}) \\ A_{ln} = \dfrac{2}{\cos(\beta_c)}\sqrt{\varphi_{\eta\eta}^{2D}(k_{\xi,l},k_{z,n})\Delta k_\xi \Delta k_z} \end{cases} \quad (2)$$

The wavenumber along the ξ axis (in Fig. 10) obeys the equation: $k_\xi = \cos(\beta_c)k_x = 2\pi f\,/\,U$. The wavenumber discretisation along the z axis is chosen arbitrarily by setting $\Delta k_z = 2\pi\,/\,L_z$ and $N = 30$ (in order to ensure 12 points per wavelength in the z direction, while injecting enough turbulent energy). In the case of the parallel gusts (defined by Eqn. (1)), the factor $\Delta k_z = 2\pi\,/\,L_z$ compensates the fact that the k_z are not defined (as detailed in [2]). The generation process is validated by comparison with the theoretical isotropic spectrum in Fig. 5.
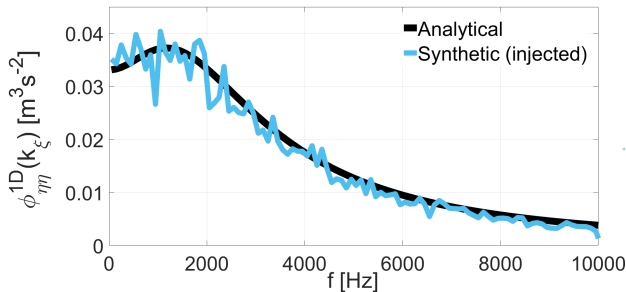

Figure 5: Velocity autocorrelation spectra (synthetic turbulence generated with a $\Delta f = 1$ Hz and averaged on 100 frequency bands).

2.4 Influence of a spanwise discretisation of the turbulence

Snapshots taken at the end of the third period are gathered in Fig. 6 and highlight the two structures of the injected turbulence. The unsteady pressure over the vane wall are then used as inputs to an in-house code (MIA), solving the loading noise term of the FWH (Ffwocs-Williams and Hawkings) equation with a free-field Green's function valid for uniform flows, in order to obtain the sound radiated in the far-field. As usually done, a simple angular average of the quadratic pressure over a rearward half circle (centred in the mid plane) is adopted for the calculation of the downstream acoustic power (PWL spectra), similarly to was is done in [12] (appendix B). Observers are placed at a distance of $r = 1.8$ m (corresponding to the microphones positions in the ECL test rig). The numerical results are compared to the Amiet formulation in Fig. 7. It is important to stress that the Amiet solution does not take into account adjacent vanes and that it considers a flat plate. First, we note a reduced radiated noise in lower frequencies which might be related to the cascade effect. A reduction can also be observed in high frequencies which is due to the airfoil thickness. Spectra from both turbulence models are almost identical which is justified analytically under certain hypothesis (high enough span-to-chord ratio and observers in the mid plane following Amiet). Finally, two bumps appear in the spectra between 2000 and 4000 Hz whose significant magnitude has not been observed in the literature [12–14]. These particular peaks are not due to statistical errors, as it is clearly demonstrated by the comparison between spectra at $\Delta f = 100$ Hz (turb. $(k_x, k_z = 0)$) and $\Delta f = 20$ Hz (turb. (k_x, k_z)). In order to understand the origin of these parasitic sources, a parametric study is performed on a simplified flat plate geometry.
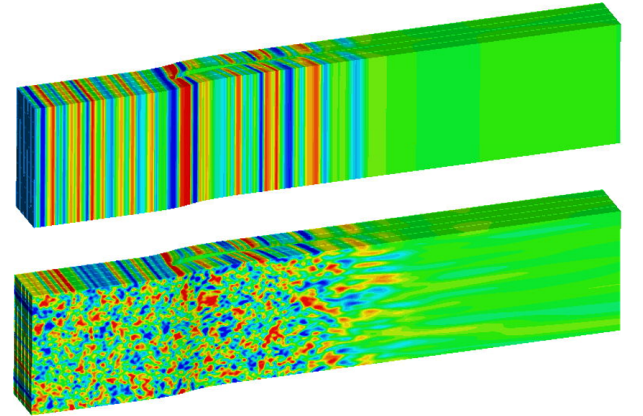

Figure 6: Snapshots of u'_y [m·s^{-1}] for the parallel (top) and oblique (bottom) gusts (levels between -2 and 2).
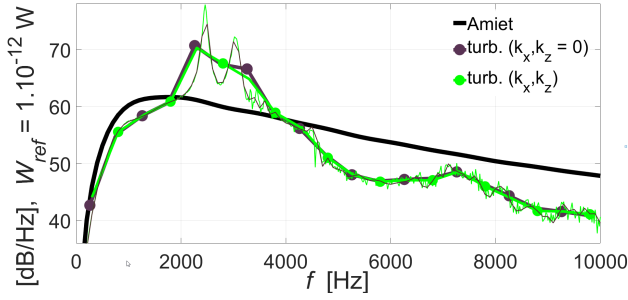
Figure 7: Downstream sound power obtained from numerical predictions and Amiet theory (isolated flat plate). Raw spectra in dashed lines and averaged (500 Hz bands) in solid lines.

2.5 Influence of flat-plate vane spacing

The parametric study is based on the pitching spacing between the flat plates. Two meshes are considered: a uniform grid (coarse mesh) and a highly refined grid around the edges (fine mesh) following criteria discussed in [2]. The different simulation domains are illustrated by Fig. 8.
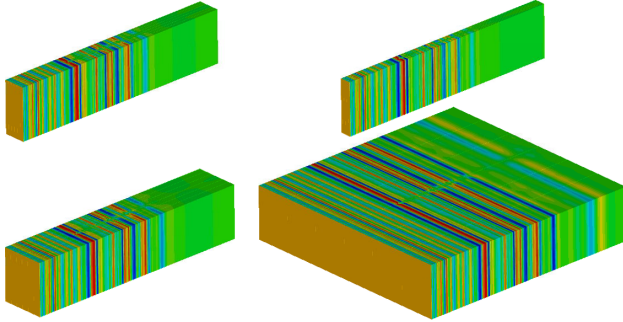

Figure 8: Snapshots of u'_y [m·s^{-1}] for various channel widths: top left ($s = 8.5$ cm), bottom left ($s = 17$ cm), top right ($s = 4.25$ cm) and bottom right ($s = 85$ cm, used to simulate free-field boundary conditions).
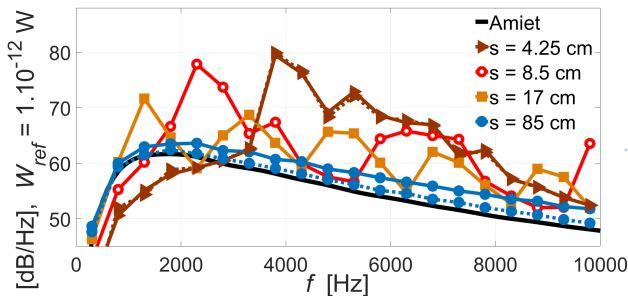

Figure 9: Donwstream sound power spectra obtained from CAA with various channel widths s. Fine meshes (for the cases $s = 4.25$ cm and $s = 85$ cm) in dashed lines.

The power spectra in the far-field are plotted in Fig. 9. First of all, it is clearly seen that the Amiet solution is retrieved for the maximum spacing value considered (s = 85 cm), which is a good point. The more the spacing is reduced, the more the bumps are getting pronounced with a peak shifted to a higher frequency. This phenomenon

can be attributed to resonance effects, as outlined by the resonance frequencies $f_R = c_0/2s$ over-plotted in Fig. 9 and close to the peaks. Hence, one can say that the present methodology cannot be applied using a single vane channel with periodicity conditions. The next section is devoted to two main extensions proposed in order to get realistic predictions:

(i) A possible decorrelation of the turbulence in the y direction through the use of a 3-wavenumber turbulence spectrum (with $k_z = 0$);

(ii) Simulations over multi channels using a 2-wavenumber or 3-wavenumber turbulence spectra.

3. MULTI CHANNELS COMPUTATIONS

3.1 Implementation of a new turbulence model

In addition to taking into account several vanes for the CAA calculation, a new turbulence formulation is implemented. This time, the k_x and k_y wavenumbers are taken into account. The k_z wavemumber has indeed shown to be of little importance in the case of non-leaned and non-swept vanes. Nevertheless, its influence on serrated airfoils will be discussed at the end of the paper. The two considered wavenumbers in the coordinate system attached to the upstream mean flow are k_ξ and k_η. The gusts frequencies can be directly connected through the dispersion relation $k_\xi = \omega / U$. As a result of the boundary conditions along the y axis, it is necessary to satisfy the following relation $k_y = n2\pi / L_y$ (with L_y the width of the domain). The wavenumber k_η is rebuilt as a linear combination of k_ξ and k_y. All variables can be visualized in Fig. 10, which facilitates the switching between the two coordinates system ((k_ξ, k_η, k_z) and (k_x, k_y, k_z)). The gusts generation follows the Eqn. (3).
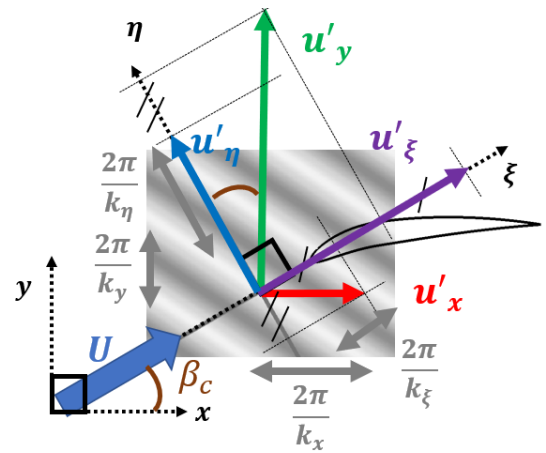

Figure 10: Schematization of the new turbulence model in both coordinate systems attached to the upstream mean flow (ξ, η, z) and reference coordinate system (x, y, z).

$$\begin{cases} \mathbf{u}' = 2\sum_{l=1}^{L}\sum_{m=-M}^{M}A_{lm}\cos(k_{\xi,l}(\xi-Ut)+k_{\eta,lm}\eta+\psi_{lm})\sigma_{\mathbf{lm}} \\[2mm] A_{lm} = \sqrt{\dfrac{E(k)}{4\pi k^2}\Delta k_{\xi}\Delta k_{\eta}\dfrac{2\pi}{L_z}} \\[2mm] (\sigma_{x,lm},\sigma_{y,lm}) = (-k_{y,m}/k, k_{x,lm}/k) \end{cases}$$

$$(3)$$

It may be observed that: $E(k) = \phi_{\eta\eta}^{3D}(k_{\xi}, k_{\eta}, k_z = 0)4\pi k^4/k_{\xi}^2$ and $E(k) = \phi_{\xi\xi}^{3D}(k_{\xi}, k_{\eta}, k_z = 0)4\pi k^4/k_{\eta}^2$. It is thus interesting to note that there is an equivalence between the two descriptions (when $k_z = 0$), using either the turbulent energy spectrum or the velocity autocorrelation spectra. The new implementation can checked through Fig. 11. The Eqn. (3) is quite similar to that given in [15].
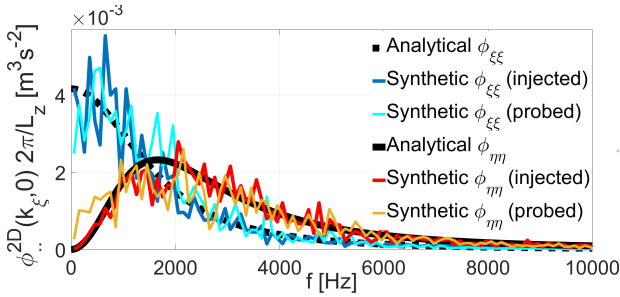

Figure 11: Velocity autocorrelation spectra (synthetic turbulence generated with a Δf = 10 Hz and averaged on 100 Hz bands). Probe is placed near the leading edge.

3.2 Parametric study on the vane count

Several simulations are performed with different vane counts. All new computations within this section are carried out with Δf = 10 Hz and averaged over 100 Hz bands.
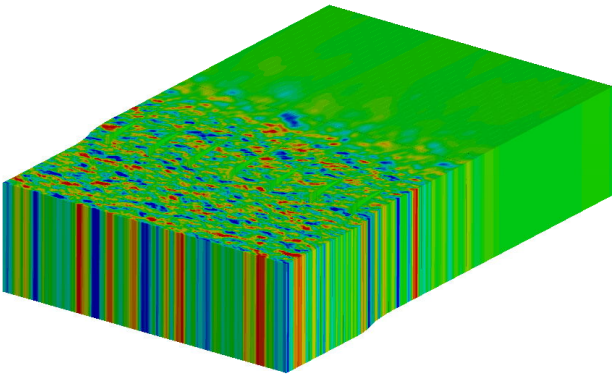

Figure 12: Snapshots of u'_y [m·s^{-1}] for the 7 vanes configuration (levels between -2 and 2).

In Fig. 13, the new turbulence implementation is also considered but this time not for a single channel domain but for a domain containing several vanes (as in Fig. 12). All the vanes of the computation are considered here for the far field propagation. There is a gap between whether
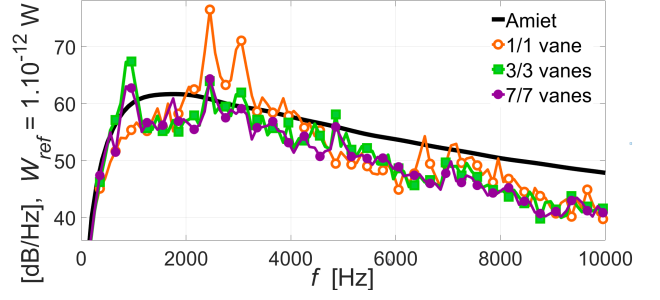

Figure 13: Downstream sound power (CAA for a different number of vanes).

or not one or several channels are considered. The greater the distance L_y is, the more there are modes k_y that are not multiples of $2\pi / s$. A decrease in the acoustic level is observed for the peaks in medium frequency for multiple channels simulations. However, one or several additional peaks appear in low frequency which seems to be due to a resonance associated with the distances multiples of s. Their amplitude diminishes as the number of vanes is increased. In [14], it has been shown that for a 20-channels computation they almost disappear. However, such a computation is expensive. A compromise between computational cost and fidelity seems to be reached when three vanes are taken into account. Fig. 14 allows us to assess the role played by the phase factor on the acoustic spectra. In particular, there is a noticeable shift in the region of the resonance bumps in medium frequency when the correlation is not taken into account for the far-field calculation. It is therefore important to take dependently all the vanes as sources for the FWH integral method. Fig. 15 compares the acoustic spectra resulting from all vanes of a 3-channels computation. The new turbulence implementation provides a smoother sound spectrum by not exhibiting bends at 4500 and 6500 Hz. However, the curve associated with the $(k_x, k_z = 0)$ turbulence does not show a significant bump in low frequency, which is due to the fact that the injected turbulence is invariant along y axis. Finally, one could conclude that the acoustic spectra in the far-field are primarily influenced by the number of vanes taken into account for the CAA computation (and the far-field propagation) rather than the structure of the turbulent spectrum.
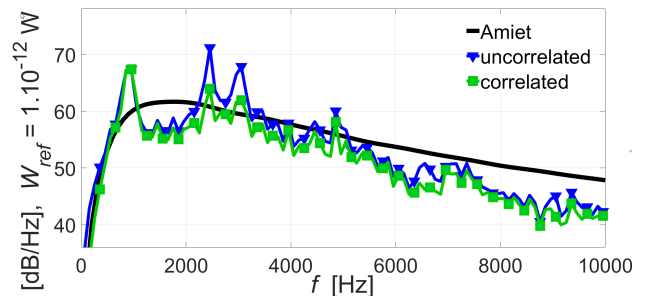

Figure 14: Downstream sound power per vane. CAA for a 3 channels computation.
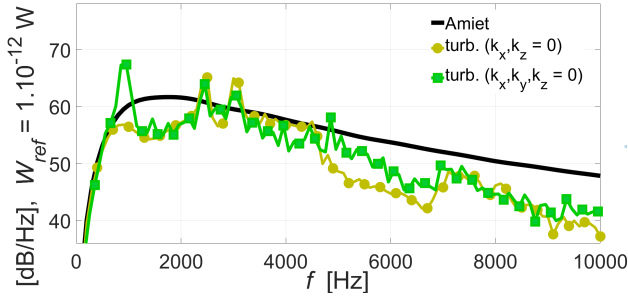
Figure 15: Downstream sound power per vane. CAA for a 3 channels computation with turbulences $(k_x, k_z = 0)$ and $(k_x, k_y, k_z = 0)$.

4. NUMERICAL ASSESSMENT OF THE NOISE REDUCTION PROVIDED BY A SERRATED LEADING EDGE

4.1 Numerical CAA Set-up

The serrations are designed following the procedure previously used at ONERA [4]. The main geometrical parameters are illustrated in Fig. 16. In particular, the serration wavelength is chosen such as $\lambda_s = 2 \cdot TLS$ and $h/\lambda_s = 1$.
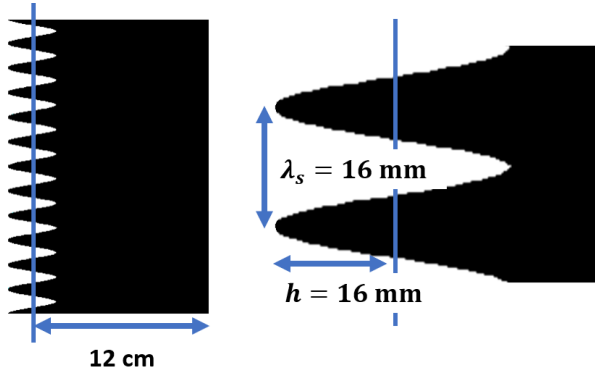

Figure 16: Geometrical parameters of the serrated design.

The mesh of the serrated vane (Fig. 17) is created by applying a transformation to the grid of the baseline (untreated) geometry. This step was achieved using an in-house tool called Ersatz (developed by R. Barrier at ONERA). However, the initial mesh had to be re-generated with a O-H pattern in order to comply with Ersatz requirements. The O-H pattern has an increased density of the mesh points around the leading edge compared to the H-Grid used previously and inversely concerning the mesh density along the y axis at the entrance. This modification of the grid pattern implies that the time step has to be reduced. A 3-channels computation (with $\Delta f = 20$ Hz) is performed on the new mesh (baseline case) and the results are compared with those provided by the previous H patterned grid. Both meshing give almost the same result as it is illustrated in Fig. 18. Only a small difference can be observed in high frequencies but, which is consistent with the fact that the new mesh is a bit more dissipative along the y axis.
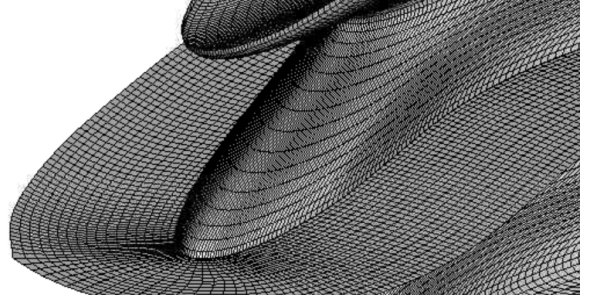

Figure 17: Zoom on slices of the serrated mesh extruded from a O-H patterned grid.
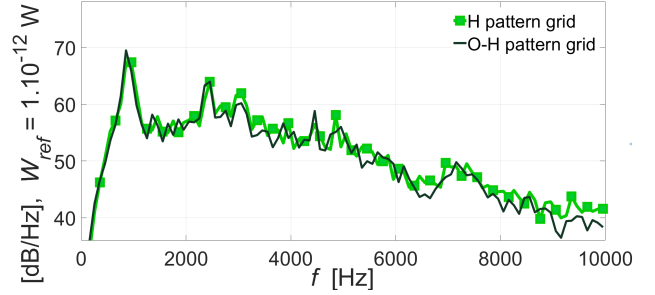

Figure 18: Downstream sound power per vane of a 3 channels computation (baseline geometry) for the H and O-H pattern meshes. Averaging over 100 Hz bands.

4.2 Mean flow computation for the serrated vane

The mean flow for the serrated geometry is computed using the same 2D Euler code than previously. In order to take into account that the geometry is no more invariant along the z axis, the mean flow is determined for each slice and interpolated over the 3D domain then. It has been shown under the scope of a previous study [4] (using a RANS mean flow), that this assumption is a good approximation as the vertical velocity is small compared to other velocity components.

4.3 Comparison of the noise reduction with analytical models

The noise reduction coming from the CAA computation will be compared with two analytical based solutions. First of all a semi-empirical law proposed by Paruchuri and discussed in [12]: $\Delta PWL = 10 \log(fh/U) + 10$. Secondly, a formulation based on the Wiener-Hopf (WH) technique proposed by Ayton et al. [10] and for which a geometrical correction has been added in [4] to take into account finite span geometries. The latter is illustrated in Fig. 19 and shows a very good agreement with the Amiet formulation for the baseline case.

The CAA computation on the serrated mesh is performed with a $\Delta f = 100$ Hz. A snapshot of the z vorticity can be seen in Fig. 20. The root mean square pressure over the vane wall is compared in Fig. 21 for both the serrated and baseline designs. In agreement with the literature, the areas of the maximal pressure are now concentrated in the roots of the serration and no more equally dis-
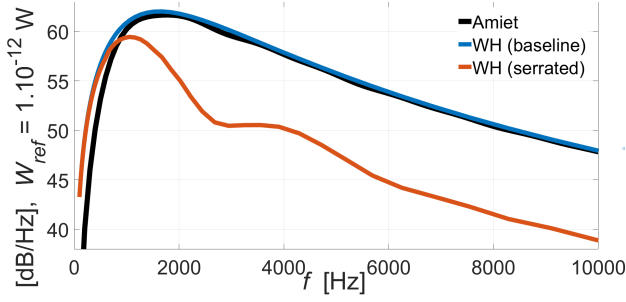
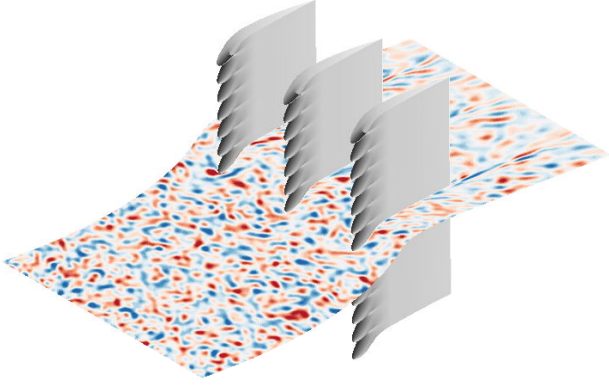**Figure 19**: Downstream sound power for an isolated flat plate with Amiet and the Wiener-Hopf technique.

Figure 20: Snapshots of ω_z' [s^{-1}] (levels between $\pm$ 750).

Figure 21: p_{RMS}' [Pa] for the baseline geometry (left) and serrated geometry (right).

Figure 22: Downstream sound power per vane for different synthetic turbulences: $(k_x, k_z = 0)$ and (k_x, k_z) (one channel computation) and $(k_x, k_y, k_z = 0)$ (3-channels computation). Baseline geometry is indicated with dashed lines and serrated geometry with solid line. A moving average over 1 kHz bands is applied.
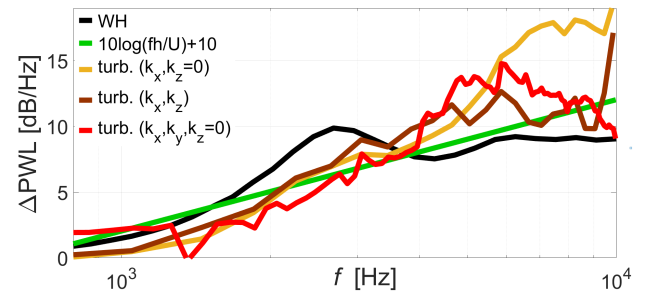
Figure 23: Downstream noise reduction for different synthetic turbulences. Analytical noise reduction coming from the Wiener-Hopf technique and law $10 \log(fh/U) + 10$.

tributed along the leading edge as in the case of the baseline geometry. Thus, a significant noise reduction can be expected. In addition to the 3-channels simulation with the new turbulence $(k_x, k_y, k_z = 0)$, two complementary simulations are carried out with the previously used synthetic turbulence methodologies. They consist in a single channel computation with parallel gusts $(k_x, k_z = 0)$ and oblique gusts (k_x, k_z). Resulting spectra can be seen in Fig. 22. A large reduction is found for all the computations with the serrated design in the medium and high-frequency ranges. In order to get a better estimation of the acoustic performances provided by the serrations, the relative noise reductions are plotted in Fig. 23. In the medium frequency ranges, all CAA computations provides a good agreement with the semi empirical law. The noise reduction seems to be a bit over estimated by the WH technique in the medium frequency range, but it has to be reminded that the analytical formulation assumes an isolated flat plate in idealistic conditions. The parallel gusts simulation overestimates the noise reduction in the high frequency range due to the fact it does not take into account oblique gusts. From the point of view of the physical phenomena associated with the noise reduction, the turbulence including the spanwise gust (k_x, k_z) provides the best fit with the empirical law, which seems to show that such a 2-wavenumber turbulence spectrum (as previously used at ONERA) might be quite relevant. As discussed in [4], it has also to be noted that the noise reduction is overestimated for all the methods in the high frequency range due to the fact the trailing edge noise is not taken into account.
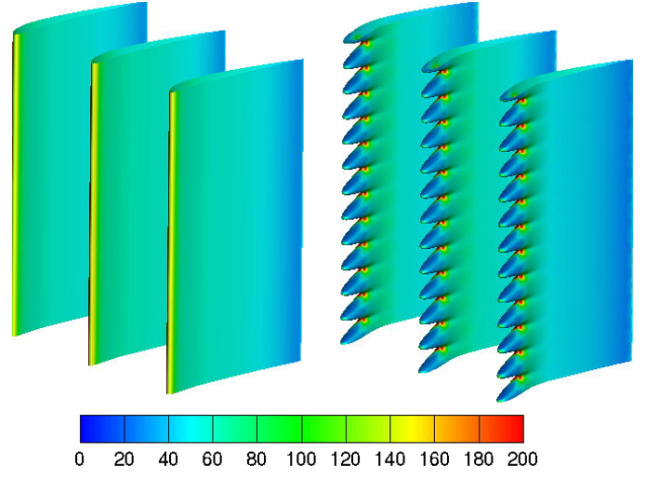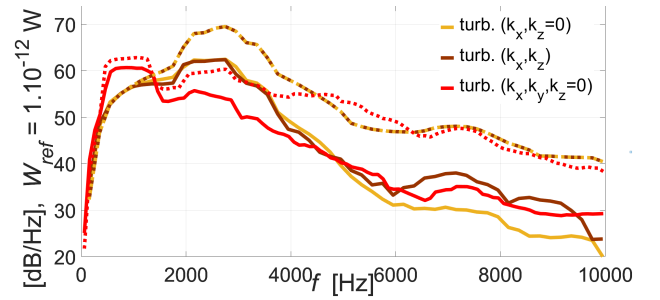
As shown in Tab. 3, the ΔOAPWL associated with the $(k_x, k_y, k_z = 0)$ turbulence is the smallest one. It is due to the overshoot in low frequencies (Fig. 22) which is linked with the resonance associated with the 3-channels periodic boundary condition. If the considered frequency range does not take into account this bump (integration of the levels from 1.3 kHz), noise reductions from CAA get much

	0 - 10 kHz	1.3 - 10 kHz
WH	5.4 dB	7.4 dB
$10 \log(St) + 10$	4.8 dB	6.4 dB
CAA $(k_x, k_z = 0)$	6 dB	6.4 dB
CAA (k_x, k_z)	6.3 dB	6.7 dB
CAA $(k_x, k_y, k_z = 0)$	3.8 dB	6 dB

Table 3: OAPWL noise reductions.

closer. Moreover, there is a small difference with the analytical formulations, which reaffirms their benefit as a very fast methodology for the noise reduction forecasting.

5. CONCLUSION

This study has highlighted some key parameters of turbulence-cascade interaction through various parametric studies. Firstly, the impact of a turbulence varying along the y direction has been investigated thanks to the implementation of a modified synthetic turbulence model. Secondly, it has been shown on the baseline configuration that multi-channel computations (at least 3 here) are mandatory to get a reliable solution, with close results using a 2-wavenumber (with $k_z = 0$) or 3-wavenumber (with $k_z = 0$) isotropic turbulence spectrum. Additionally, the noise reduction associated with a serrated leading edge has been assessed using the new methodology. In accordance with the best practices issued from the parametric studies on the baseline configuration, a 3-channels simulation has been performed in order to determine the noise radiated by vanes with a serrated leading edge. If one is only interested in the relative noise reduction, a single channel simulation has shown to be sufficient (especially as the k_z discretization is taken into account). Moreover, it has been also demonstrated experimentally in [12], that the noise reductions are close to the theoretical solution regardless of the number of vanes taken into account. However, a multi-channel computation is of prime importance in order to accurately estimate the absolute noise level. Moreover, the extension of the simulation using a fully 3D synthetic turbulence (k_x, k_y, k_z) will be the object of a future communication. Finally, the Wiener-Hopf technique has been successfully applied in order to be compared with the numerical results along with a semi-empirical law $10 \log(fh/U) + 10$. All three provided a good agreement for prediction of the overall noise reduction, which is a major step and key result obtained from the present study.

6. REFERENCES

[1] A. Finez, *Etude expérimentale du bruit de bord de fuite à large bande d'une grille d'aubes linéaire et de sa réduction par dispositifs passifs*. PhD thesis, Ecole centrale de Lyon, France, 2012.

[2] V. Clair, *Calcul numérique de la réponse acoustique d'un aubage soumis à un sillage turbulent*. PhD thesis, Ecole centrale de Lyon, France, 2013.

[3] C. Polacsek, V. Clair, T. Garrec, G. Reboul, and M. Jacob, "Numerical predictions of turbulence/cascade-interaction noise using computational aeroacoustics with a stochastic model," *AIAA Journal*, vol. 53, pp. 1–16, 10 2015.

[4] C. Polacsek, A. Cader, M. Buszyk, R. Barrier, F. Gea-Aguilera, and H. Posson, "Aeroacoustic design and broadband noise predictions of a fan stage with serrated outlet guide vanes," *Physics of fluids*, vol. 32, no. 10, p. 107107, 2020.

[5] R. Kraichnan, "Diffusion by a random velocity field," *Physics of Fluids*, vol. 13, pp. 22–31, 1970.

[6] W. Bechara, C. Bailly, P. Lafon, and S. Candel, "Stochastic approach to noise modeling for free turbulent flows," *AIAA Journal*, vol. 32, pp. 455–463, 1994.

[7] J. Blazek, *Computational Fluid Dynamics 3rd Edition. Principles and Applications.* Germany: Butterworth-Heinemann, 2015.

[8] G. Reboul, *Modélisation du bruit à large bande de soufflantes de turboréacteurs*. PhD thesis, Ecole centrale de Lyon, France, 2010.

[9] C. Cheong, P. Joseph, and S. Lee, "Frequency formulation for the acousticpower spectrum due to cascade-turbulence interaction," *The Journal of the Acoustical Society of America*, vol. 119, pp. 108–22, 2006.

[10] L. Ayton and C. Paruchuri, "An analytical and experimental investigation of aerofoil–turbulence interaction noise for plates with spanwise-varying leading edges," *Journal of Fluid Mechanics*, vol. 865, pp. 137–168, 2019.

[11] A. Cader, C. Polacsek, T. L. Garrec, R. Barrier, F. Benjamin, and M. Jacob., "Numerical prediction of rotor-stator interaction noise using 3d caa with synthetic turbulence injection," in *Proc. of the AIAA/CEAS Aeroacoustics Conference*, (Atlanta, United States), 2018.

[12] L. Mazella, C. Paruchuri, G. Lacagnina, Y. Mao, and P. Joseph, "Experimental investigation of the noise control performance of leading edge serrations in a rectilinear cascade," in *Proc. of the AIAA/CEAS Aeroacoustics Conference*, (Delft, The Netherlands), 2019.

[13] V. Blandeau, P. Joseph, G. Jenkins, and C. Powles, "Comparison of sound power radiation from isolated airfoils and cascades in a turbulent flow," *The Journal of the Acoustical Society of America*, vol. 129, pp. 3521–30, 2011.

[14] F. Gea-Aguilera, *Aerodynamic and aeroacoustic modelling of engine fan broadband noise*. PhD thesis, University of Southampton, England, 2017.

[15] F. Gea-Aguilera, X. Zhang, X. Chen, and J. Gill., "Synthetic turbulence methods for leading edge noise predictions," in *Proc. of the 21st AIAA/CEAS Aeroacoustics Conference*, (Dallas, United States), 2015.